Aging and clustering in globally coupled oscillators

Hiroaki Daido* and Kenji Nakanishi†
Department of Mathematical Sciences, Graduate School of Engineering, Osaka Prefecture University, Sakai 599-8531, Japan
(Received 13 November 2006; published 10 May 2007)

A population of coupled nonlinear oscillators may age in such a way that the fraction of non-self-oscillatory elements increases. Following our previous paper [Phys. Rev. Lett. **93**, 104101 (2004)], we study the effect of aging in this sense mainly for globally coupled Stuart-Landau oscillators with the emphasis on the structure of the (K,p) phase diagram, where K is the coupling strength and p is the ratio of inactive oscillators. In addition to the aging transition reported previously, such a diagram is shown to be characterized by a hornlike region, which we call a "desynchronization horn," where active oscillators desynchronize to form a number of clusters, provided that uncoupled active oscillators are sufficiently nonisochronous. We also show that desynchronization in such a region can be captured as a type of diffusion-induced inhomogeneity based on a "swing-by mechanism." Our results suggest that the desynchronization horn with some curious properties may be a fairly common feature in aging systems of globally and diffusively coupled periodic oscillators.

DOI: 10.1103/PhysRevE.75.056206 PACS number(s): 05.45.Xt, 87.10.+e, 05.45.−a

I. INTRODUCTION

Coupled nonlinear oscillators appear in a variety of areas in science and technology. In particular, the behavior of their large populations has been one of the central research subjects since Winfree's pioneering work in the late 1960's [1]. This is because detailed knowledge about the dynamics and statistical-mechanical properties of such large-scale dynamical systems is indispensable in those areas. For example, the concept of macroscopic synchronization established by quite a few theoretical studies [2–5] plays a crucial role in explaining a rich variety of coherent activities of coupled oscillatory elements observed in diverse areas. This variety includes, on the one hand, many important activities of living organisms to maintain life, e.g., heart contraction, peristaltic motion of gastrointestinal tracts, circadian rhythms [6], and visual information processing in mammalian brains [7] and, on the other hand, synchronous behavior of myriads of inorganic systems treated in more conventional physics and engineering such as coupled Josephson junctions and coupled electrochemical oscillators [8–11].

As exemplified above, biological or physiological systems are often regarded as large populations of coupled oscillators. However, needless to say, any living system cannot avoid some form of deterioration which may be caused by aging and accidental events such as disease. If the level of such deterioration becomes higher than a certain critical threshold, the function of a physiological oscillator system will be lost and its host organism may be brought to a serious illness or death. It is therefore important to ask how robust the activity or performance of the system can be against such deterioration. This problem is equally important in technological contexts, where it is crucial to design robust systems. Nevertheless, there have been few studies devoted to it so far.

Motivated by this problem, in a previous paper [12] (see also Ref. [13]), the authors discussed the behavior of globally and diffusively coupled nonlinear oscillators such that some of them are active (i.e., self-oscillatory) oscillators while others are inactive (i.e., non-self-oscillatory) oscillators. In this work, as well as the present, the ratio of the latter, denoted by p, stands for the level of aging or deterioration of the system, and we deal with equilibrium properties of the system for each fixed value of p. Hence, in view of the context of aging in its literal sense, our work will correspond to studying the slow-progress limit of aging. We consider this as a convenient starting point for our study. In an earlier paper [12], it was found that as the ratio p exceeds a critical value, p_c, the system loses its oscillatory activity to fall in a steady state. What is remarkable is that the critical ratio p_c becomes less than unity when the strength of coupling among oscillators K is larger than a threshold value K_c. Such a transition between activity and inactivity of the population at $p=p_c<1$ was called an aging transition. The value of p_c tends to decrease for increasing K in the range $K>K_c$. As pointed out in Ref. [12], one important implication of this result is that although strong coupling among oscillators generally helps to maintain the system's coherence, it can also spoil the robustness of the system's activity against aging or deterioration in the sense considered here. This might suggest the possibility that the intensity of coupling in living coupled-oscillator systems is tuned to an optimal value. The aging transition is a critical phenomenon, for which a natural order parameter is

$$M \equiv \sqrt{\langle (\mathbf{X}_c - \langle \mathbf{X}_c \rangle)^2 \rangle}, \tag{1}$$

where $\mathbf{X}_c$ is the centroid of the state vectors of all oscillators and the brackets mean long time average. It was also shown in Ref. [12] that this order parameter, which measures the oscillatory activity of the system as a whole, obeys some universal scaling laws near the aging transition and also near the critical point, i.e., $(K,p)=(K_c,1)$. It is important to note that these results do not depend on whether active oscillators are periodic or chaotic [12,13]. Quite recently, our frame-

*Author to whom correspondence should be addressed.
†Present address: Hitachi Medical Corporation, Research Development Center, 2-1, Shintoyofuta, Kashiwa, Chiba, 277-0804 Japan.

work of aging study for coupled oscillators has been applied to neuronal models [14].

In this paper, following the earlier, we investigate the effect of aging on the dynamics of globally and diffusively coupled oscillators with the emphasis on the desynchronization of active oscillators. It was already reported [12,13] that in some region of the (K,p) phase diagram, active oscillators split into a number of clusters, though all inactive oscillators empirically seem to be synchronized everywhere in the phase diagram. We shall elucidate the nature of such desynchronization or clustering analytically as well as numerically. For brevity, we focus on the case that active elements of the system are identical limit-cycle oscillators. Moreover, we only deal with the scalor type of diffusive coupling. The paper is organized as follows. In Sec. II, which constitutes the main body of this article, the case of coupled Stuart-Landau oscillators will be discussed in detail. The Stuart-Landau system is a normal form describing dynamics near Hopf bifurcation [2]. We therefore expect that the results of this section will be applicable at least to populations of oscillators near Hopf bifurcation. Some of the results of this section were reported elsewhere [15]. In Sec. III, we will examine the behavior of populations of other oscillators to check if the results of Sec. II can be in fact more general. Finally, in Sec. IV, this paper will be summarized with discussion about the significance of our results and remaining problems. All numerical simulations reported below were performed with the fourth order Runge-Kutta method with time step 0.1 or smaller.

II. COUPLED STUART-LANDAU OSCILLATORS

This section, which is the main part of this article, is devoted to a study of the behavior of the following dynamical system [12]:

$$\dot{z}_j = (\alpha_j + i\Omega)z_j - (1 + ic_2)|z_j|^2 z_j + \frac{K}{N}\sum_{k=1}^{N}(z_k - z_j) \qquad (2)$$

for $j=1,\ldots,N$, where the overdot means differentiation with respect to time t, z_j is the complex amplitude of the jth oscillator, α_j is a parameter specifying the distance from Hopf bifurcation, Ω is the natural frequency, c_2 is a parameter controlling the degree of nonisochronicity (i.e., amplitude dependency of the angular frequency), and $K>0$ is the coupling strength. For $K=0$, the jth element exhibits periodic oscillation if $\alpha_j>0$, and settles down at the trivial fixed point $z_j=0$ if $\alpha_j \leqslant 0$. We assume that aging of the system proceeds in such a way that an active oscillator with $\alpha_j=a>0$ turns inactive with $\alpha_j=-b<0$, where both a and b are parameters. The system size N will be supposed to be large enough to enable us to regard the ratio of inactive elements p virtually as a continuous variable. For convenience, we set the group of active elements to $j \in \{1,\ldots,N(1-p)\} \equiv S_a$ and that of inactive elements to $j \in \{N(1-p)+1,\ldots,N\} \equiv S_i$. The $p=0$ version of Eq. (2) with K either complex or real was studied in a number of papers [16–21] and shown to exhibit a variety of behaviors such as synchronization, incoherence, clustering, and chaos.

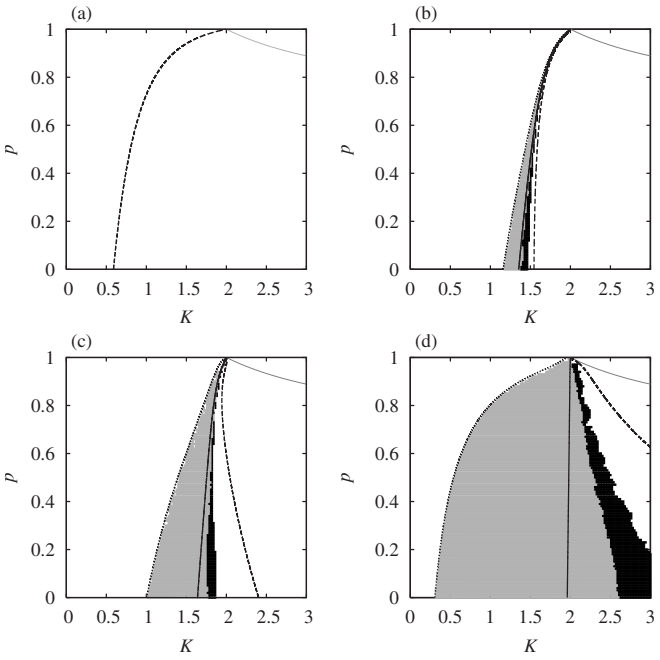

FIG. 1. Phase diagrams for several values of c_2: (a) −0.5, (b) −2, (c) −3, (d) −10. The colored regions are where the active group of the system with $N=1000$, $a=2$, $b=1$ was numerically found to be desynchronized; the state is either periodic (dark) or nonperiodic (gray). The thin dotted curve lying at the right upper corner of each panel is the aging transition line given by Eq. (3), above which the death state is stable. The dashed, solid, and dotted curves converging at $(K,p)=(2,1)$ show theoretical curves corresponding to K_{SN}, K_H, and K_{SC}, respectively (see the text for details).

A. Phase diagrams

Figure 1 shows phase diagrams with respect to parameters K and p for several values of c_2. The simulation results displayed therein were obtained for a random initial condition taken in the range $-1<\mathrm{Re}\, z_j, \mathrm{Im}\, z_j<1$ $(j=1,\ldots,N)$. Note that as can be seen by taking complex conjugate of Eq. (2), this kind of phase diagram does not depend on the sign of c_2. In each panel, we find both active and inactive regions: In the former, all elements of the system oscillate with amplitudes which are larger for active elements than for inactive elements, while in the latter, the system is in the death state with $z_j=0$ for all j. The aging transition occurs at the boundary between these regions, which is given, irrespective of c_2, by [12]

$$p = \frac{a(K+b)}{(a+b)K} \quad (K \geqslant a) \qquad (3)$$

as drawn in the panels of Fig. 1. Hence, the critical ratio p_c is given by the right-hand side of Eq. (3) for $K>a$, whereas $p_c=1$ for $K \leqslant a$. This result implies that $K_c=a$ in the present model. Moreover, we see that for $K>K_c$, p_c monotonically decreases for increasing K. As mentioned in the previous section, this behavior of p_c implies that as the interaction is intensified, the population of coupled identical Stuart-Landau oscillators becomes more and more fragile against aging.

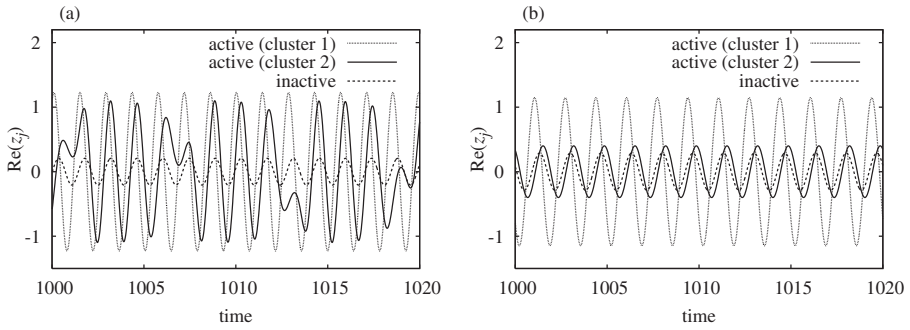

FIG. 2. Examples of time series data for $N=1000$, $c_2=-3$, $a=2$, $b=1$, $p=0.4$. Here we have three synchronized clusters: the larger active (cluster 1), the smaller active (cluster 2), and the inactive. (a) $K=1.32$ (quasiperiodic state; the size of cluster 2 is 2). (b) $K=1.82$ (periodic state; the size of cluster 2 is 27).

In Fig. 1 we also find that for $|c_2|$ large, the active region is divided into two regions: One is the region where both active and inactive groups of the population synchronize within each and the other is the one in which only the group of active elements desynchronize to split into more than one cluster. Although the latter region slightly varies from one initial condition to another, its basic shape reminiscent of a horn converging at $(K,p)=(K_c,1)$ remains qualitatively the same for random initial conditions of the type chosen here. Inspired by its characteristic shape, we call such a region a "desynchronization horn." In fact, according to our numerical results, the state in which the active group, as well as the inactive, is synchronized seems to be stable everywhere in the checked region of the phase diagram (up to $K=2K_c$). Each numerically found desynchronized horn should therefore be part of a probably bigger region where both the perfectly synchronized state and a number of desynchronized states stably coexist in phase space. We remark that as Fig. 1 indicates, the horn grows for increasing $|c_2|$. Hereafter, we will use the term "desynchronization" and other related ones in order to mean the desynchronization of the active group for simplicity.

Let us now check the behavior of the system in more detail. Figure 2 displays a pair of examples of time-series data in a desynchronized horn. Desynchronized solutions tend to be periodic near the right boundary and quasiperiodic near the left boundary. In either case, the active group typically consists of two clusters such that one of them is overwhelmingly larger in size than the other. Figure 2(a) shows an example of quasiperiodic solution found near the left boundary of a desynchronized horn, while Fig. 2(b) is devoted to an example of periodic two-cluster solutions observed near the right boundary. The variety of solutions found away from the boundaries is more complex and depends on initial conditions. Figure 3 presents an example of cluster structures of the active group over a whole range of K across a horn for a fixed value of p. This figure shows that the number of clusters in the active group tends to be much larger near the center than near the boundaries of the range. Moreover, we found that for some values of K in the central region, the configuration of the active group failed to become stationary within the time interval used for computation (10^4). It seems very difficult to explain all the aspects of this complex clustering dynamics [5,22,23], but some features of the horn as well as the mechanism of the appearance of such inhomogeneous states can be theoretically approached, as discussed in the coming subsections.

B. Two-cluster desynchronization in the small size-ratio limit

In this subsection, we analytically study the behavior of the system in the desynchronization horn by restricting ourselves to the simplest category of clustering of the active group. Let us start by supposing that the active group consists of two synchronized clusters with size ratio $r:1-r$ ($0<r\leqslant 1/2$), while the inactive group is synchronized. We then have totally three clusters with sizes $r(1-p)N$, $(1-r)\times(1-p)N$, and pN. Writing their complex amplitudes u,v,w in the same order, we obtain from Eq. (2)

$$\dot{u}=[a-K+Kr(1-p)]u-(1+ic_2)|u|^2u + K(1-r)(1-p)v+Kpw, \tag{4}$$

$$\dot{v}=[a-K+K(1-r)(1-p)]v-(1+ic_2)|v|^2v + Kr(1-p)u+Kpw, \tag{5}$$

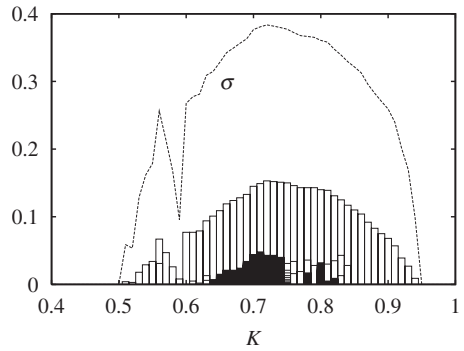

FIG. 3. Cluster structures of numerically found solutions for a random initial condition and $N=1000$, $c_2=-3$, $a=b=1$, $p=0$. Each segment of a vertical bar shows the size ratio of a cluster smaller than the main cluster, which is not shown here. These segments are placed in the order of their sizes, from top to bottom. Almost black regions correspond to the existence of a large number of small clusters. A cluster here is defined to be a collection of oscillators less than 10^{-5} apart from one oscillator at $t=10\,000$. The behavior of σ defined in Eq. (41) is also shown.

$$\dot{w} = [-b - K + Kp]w - (1 + ic_2)|w|^2 w + Kr(1-p)u + K(1-r)(1-p)v, \tag{6}$$

where and hereafter the natural frequency Ω is set to be zero without loss of generality. By taking the limit $r \to 0$, these equations are simplified as

$$\dot{u} = (a - K)u - (1 + ic_2)|u|^2 u + K(1-p)v + Kpw, \tag{7}$$

$$\dot{v} = (a - Kp)v - (1 + ic_2)|v|^2 v + Kpw, \tag{8}$$

$$\dot{w} = [-b - K + Kp]w - (1 + ic_2)|w|^2 w + K(1-p)v. \tag{9}$$

As we see in these equations, both v and w evolves independently of u, which is why this limit is tractable. As a matter of fact, their equations are nothing but those for the synchronized state. In this subsection, we concentrate on the reduced system (7)–(9). The results obtained below will be used to approximately describe two-cluster states of the active group with $0 < r \ll 1$, for example, when the size of the smaller active cluster is $O(N^s)$ with $s < 1$, since the system size N is assumed to be large in this paper.

In the following, the behavior of the reduced system (7)–(9) will be discussed separately for the three cases: $p = 0$, $0 < 1 - p \ll 1$, and the rest. The main results for case (a) below were already reported in Ref. [15].

(a) *The case of* $p = 0$. In this case, the population is composed only of identical active elements. For simplicity, we set $a = 1$. This simplification can be achieved without damaging the generality of our argument by the transformations

$$z_j \to \sqrt{a} z_j, \quad t \to t/a, \quad K \to Ka. \tag{10}$$

We first note that in this case, v obeys the equation of the uncoupled active oscillator, i.e.,

$$\dot{v} = v - (1 + ic_2)|v|^2 v. \tag{11}$$

This equation possesses a globally stable limit-cycle solution expressed as

$$v = \exp\{i(-c_2 t + \text{const})\} \equiv v_p(t). \tag{12}$$

Then, the u-independent term in Eq. (7) for $p = 0$ will act as a periodic external force on the dynamics of the smaller cluster. In order to study its behavior conveniently, we introduce $\tilde{u} \equiv u/v_p(t)$ to obtain

$$\dot{\tilde{u}} = [(1 - K) + ic_2]\tilde{u} - (1 + ic_2)|\tilde{u}|^2 \tilde{u} + K, \tag{13}$$

except for an initial transient in which the larger cluster does not yet settle on the limit cycle.

It is easy to see that the last equation has a fixed point $\tilde{u} = 1$ for all K, which corresponds to the perfectly synchronized state, $u = v$. The stability of this fixed point under Eq. (13) is governed by the following eigenvalue equation:

$$\lambda^2 + 2(1 + K)\lambda + K(K + 2) = 0, \tag{14}$$

which gives $\lambda = -K, -(K+2)$, so that the fixed point is stable, regardless of the values of K and c_2.

It can also be shown that the dynamical system (13) has a pair of other fixed points if $K < K_{\mathrm{SN}}$, where

$$K_{\mathrm{SN}} \equiv \frac{1 + c_2^2}{2(1 + \sqrt{1 + c_2^2})} \tag{15}$$

is their saddle-node bifurcation point. Those fixed points, which represent desynchronized periodic states in terms of the original variables, are given by

$$\tilde{u}_\pm \equiv \frac{K}{K + (1 + ic_2)y_\pm} \tag{16}$$

with

$$y_\pm \equiv \frac{-(2K + 1 + c_2^2) \pm \sqrt{(2K + 1 + c_2^2)^2 - 4(1 + c_2^2)K(K+2)}}{2(1 + c_2^2)}.$$

Let $\mathbf{J}_\pm$ be Jacobi matrices obtained by linearizing Eq. (13) about the fixed points $\tilde{u}_\pm$. Some algebra yields

$$\det \mathbf{J}_\pm = 2K(K+2)\left[\frac{2K + 1 + c_2^2}{2K + 1 + c_2^2 \pm \sqrt{(2K + 1 + c_2^2)^2 - 4(1 + c_2^2)K(K+2)}} - 1\right], \tag{17}$$

which reveals that $\tilde{u}_+$ is always a saddle, while $\tilde{u}_-$ is either a node or a focus. The stability of the fixed point $\tilde{u}_-$ can be determined with the aid of the following formula:

$$\frac{1}{2}\mathrm{tr}\mathbf{J}_- = \frac{1 - c_2^2}{1 + c_2^2}K + \frac{\sqrt{(2K + 1 + c_2^2)^2 - 4(1 + c_2^2)K(K+2)}}{1 + c_2^2}, \tag{18}$$

where "tr" stands for trace. Namely, for $|c_2| < 1$, $\tilde{u}_-$ is always unstable, since $\mathrm{tr}\mathbf{J}_- > 0$ in that case. On the other hand, for $|c_2| > 1$, there appears an interval of K in which $\tilde{u}_-$ is stable, which is the interval $K_H < K < K_{\mathrm{SN}}$, where

$$K_H \equiv \frac{-2 + \sqrt{4 + (1 + c_2^2)^2}}{1 + c_2^2}. \tag{19}$$

Actually, $K = K_H$ is a Hopf bifurcation point: as K passes K_H from above, a stable limit-cycle appears following destabilization of the fixed point $\tilde{u}_-$ at $K = K_H$. In view of the original variables, this means the onset of quasiperiodicity as exemplified in Fig. 2(a). Numerical integration of Eq. (13)

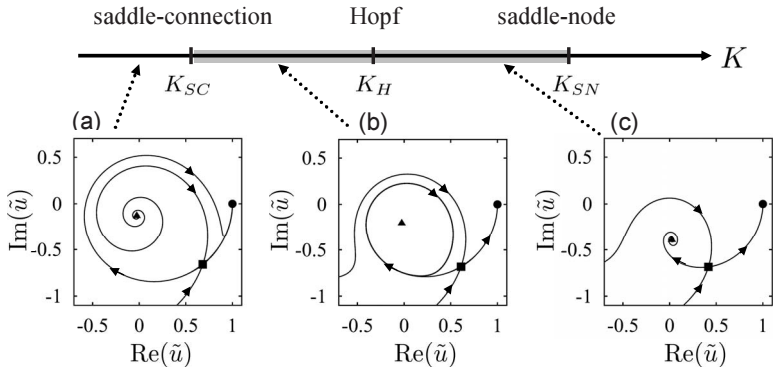

FIG. 4. Phase portraits on $(\mathrm{Re}\tilde{u}, \mathrm{Im}\,\tilde{u})$ plane of the system (13) with $a=b=1$, $c_2=-3$, where the critical values of K are approximately given by $K_{\mathrm{SC}}=0.502$, $K_H=0.820$, and $K_{\mathrm{SN}}=1.201$. In each panel, the circle ($\tilde{u}=1$) is a stable fixed point corresponding to the synchronized state and the square ($\tilde{u}_+$ in text) is a saddle, whose stable and unstable manifolds are also shown. The fixed point marked by the triangle ($\tilde{u}_-$ in text) represents a desynchronized periodic state, being stable only in panel (c). In panel (b), a stable limit cycle is also displayed, which may be interpreted as a desynchronized quasiperiodic state.

indicates that as K is further decreased, the limit cycle grows in its amplitude and eventually collides with the saddle $\tilde{u}_+$ at some value of K, say K_{SC}, to form a saddle connection and disappear for $K<K_{\mathrm{SC}}$. This bifurcation scenario is illustrated in Fig. 4. For $K<K_{\mathrm{SC}}$, no desynchronized attractors exist and the active group exhibits only perfect synchronization expressed by the trivial fixed point $\tilde{u}=1$.

We remark that according to Eqs. (15) and (19), $K_H=K_{\mathrm{SN}}=\sqrt{2}-1$ for $|c_2|=1$. Since no Hopf bifurcation occurs and hence no limit cycles appear for $|c_2|<1$, K_{SC} should also converge to the same value for $|c_2|\to 1+0$. In fact, the curve of K_{SC} drawn numerically in Fig. 5 together with those of K_{SN} and K_H due to Eqs. (15) and (19) seems to support this conjecture. Figure 5 also displays a region where a desynchronized state appears for a random initial condition. Its left boundary is found to be nicely approximated by the curve of K_{SC}, while its right boundary is situated far away from the curve of K_{SN}. The latter fact will be explained later in Sec. II C. We may also note that the boundary between periodicity and nonperiodicity substantially deviates from the curve of K_H, which is no wonder because cluster structures in the central region typically differ from the one supposed here (see Fig. 3).

(b) *The case of* $(K,p)\sim(K_c,1)$. Here we investigate the behavior of u under the assumption that (K,p) is in the active region $(p<p_c)$ and close to $(K_c,1)=(a,1)$. For this purpose, we first pay attention to the solution of Eqs. (8) and (9). Since we have taken the small size-ratio limit, it describes the behavior of the system when the active group, as well as the inactive, is synchronized. Suggested by our numerical results mentioned before, we assume that after a transient period, it is attracted to a stable periodic solution

$$v = Ae^{i\omega t}, \quad w = Ie^{i\omega t}, \tag{20}$$

where amplitudes A, I and frequency ω are all constants [24]. Substituting these expressions into Eqs. (8) and (9) and setting $A\neq 0$, we obtain the following equations:

$$I = f(|A|^2,\omega)A, \tag{21}$$

$$[b+K(1-p)+i\omega]f(|A|^2,\omega) + (1+ic_2)|f(|A|^2,\omega)|^2|A|^2 f(|A|^2,\omega) = K(1-p), \tag{22}$$

where

$$f(x,\omega) \equiv \frac{-a+Kp+i\omega+(1+ic_2)x}{Kp}.$$

Equation (22) determines the amplitude $|A|$ as well as the frequency ω through its real and imaginary parts. We then replace (v,w) in Eq. (7) by this periodic solution and, for convenience, make a transformation from u to $U\equiv ue^{-i\omega t}$ to find

$$\dot{U} = (a-K-i\omega)U - (1+ic_2)|U|^2U + K\{(1-p)A+pI\}. \tag{23}$$

It should be noted that these equations (20)–(23) are not restricted to the particular case $(K,p)-(a,1)$ addressed below. It is also crucial to keep in mind that the last equation

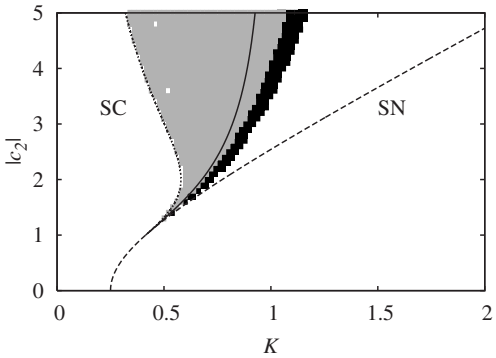

FIG. 5. Phase diagram for K and $|c_2|$ based on the approximation developed in the text for $p=0$, $a=b=1$, where the rightmost, middle, leftmost curves show $K=K_{\mathrm{SN}}, K_H, K_{\mathrm{SC}}$, respectively. The dark and gray areas are where numerical simulation of Eq. (2) starting from a random initial condition produced desynchronized periodic and nonperiodic solutions, respectively.

always has $U=A$ as a fixed point, which corresponds to the synchronization of all active oscillators.

Let us now introduce a pair of small parameters $\delta \equiv 1-p$ and $\mu \equiv K_c - K = a - K$. It is straightforward to realize from Eq. (22) or more directly from Eqs. (8) and (9) that the frequency ω as well as the amplitudes A and I vanish for $\delta = \mu = 0$. Going a step forward, we obtain

$$\omega = -c_2\mu - c_2 a\left(1+\frac{a}{b}\right)\delta + \cdots, \tag{24}$$

$$A^2 = \mu + a\left(1+\frac{a}{b}\right)\delta + \cdots, \tag{25}$$

where A has been taken to be real without harming the generality of our argument, and the discarded terms are of the second order as to the small parameters. Making use of these results and introducing

$$\tilde{U} \equiv \frac{U}{\sqrt{a\left(1+\frac{a}{b}\right)\delta}}, \tag{26}$$

$$\tau \equiv a\left(1+\frac{a}{b}\right)\delta t, \tag{27}$$

$$d \equiv \frac{\mu}{a\left(1+\frac{a}{b}\right)\delta}, \tag{28}$$

and finally taking the limit $\delta \to 0$ with d fixed, we obtain

$$\frac{d\tilde{U}}{d\tau} = \{(1+ic_2)d + ic_2\}\tilde{U} - (1+ic_2)|\tilde{U}|^2\tilde{U} + \sqrt{1+d}, \tag{29}$$

which describes the asymptotic dynamics of u near the critical point $(K,p)=(K_c,1)$ by way of

$$u = Ue^{i\omega t} = \sqrt{a\left(1+\frac{a}{b}\right)\delta}\,\tilde{U}e^{i\omega t}. \tag{30}$$

Below we study fixed points of Eq. (29) and their bifurcations using d as the control parameter. Critical values of d will then give, via Eq. (28), critical slopes of corresponding bifurcation curves at $(K,p)=(K_c,1)$.

First of all, it is worth noting that any fixed point of the dynamical system (29) must satisfy

$$\tilde{U} = \frac{\sqrt{1+d}}{|\tilde{U}|^2 - d + ic_2\{|\tilde{U}|^2 - (1+d)\}}. \tag{31}$$

Moreover, it is easy to derive the formulas

$$\mathrm{tr}(\mathbf{J}) = 2(d - 2|\tilde{U}|^2), \tag{32}$$

$$\det(\mathbf{J}) = 3(1+c_2^2)|\tilde{U}|^4 - 4\{d + (1+d)c_2^2\}|\tilde{U}|^2 + d^2 + c_2^2(1+d)^2, \tag{33}$$

where $\mathbf{J}$ is the Jacobi matrix at the fixed point. There are at most three fixed points with the system (29). By inspection, we see that one of them is given by $\tilde{U}=\sqrt{1+d}$, which corresponds to perfect synchronization $(U=A)$, as can be shown using Eqs. (25), (26), and (28). It is easy to see that this fixed point is stable as long as it exists, i.e., for $d \geqslant -1$. We remark that $d=-1$ gives the critical slope of the aging transition curve given by Eq. (3), as it should be.

Other fixed points corresponding to clustering of the active group may be found from the following equation which is obtained by taking the absolute values of both sides of Eq. (31) and then defactorizing $|\tilde{U}|^2-(1+d)$:

$$F(|\tilde{U}|^2) \equiv (1+c_2^2)|\tilde{U}|^4 + \{2 - (1+c_2^2)(1+d)\}|\tilde{U}|^2 + 1 = 0. \tag{34}$$

An analysis of this equation shows that there exists a couple of new fixed points $\tilde{U}_\pm$ for $d > d_{\mathrm{SN}}$, where

$$d_{\mathrm{SN}} \equiv \frac{1 - c_2^2 + 2\sqrt{1+c_2^2}}{1+c_2^2} \tag{35}$$

is their saddle-node bifurcation point and

$$|\tilde{U}_\pm|^2 = \frac{(1+c_2^2)(1+d) - 2 \pm \sqrt{\{(1+c_2^2)(1+d)-2\}^2 - 4(1+c_2^2)}}{2(1+c_2^2)}. \tag{36}$$

Let us find out about the types and stability of these fixed points. For this purpose, we need to know the signs of the determinants of their Jacobi matrices $\mathbf{J}_\pm$. First of all, from Eqs. (33) and (34), we obtain

$$\det(\mathbf{J}_\pm) = \{(1+c_2^2)(1+d) + 2\}\{V - |\tilde{U}_\pm|^2\}, \tag{37}$$

where

$$V \equiv \frac{d^2 + c_2^2(1+d)^2 - 3}{(1+c_2^2)(1+d)+2}.$$

By some tedious but simple calculations, we also obtain

$$F(V) = -\frac{y\{f_1 y^2 + f_2 y + f_3\}}{\{(1+c_2^2)(1+d)+2\}^2}, \tag{38}$$

where F is defined in Eq. (34) and $y \equiv (1+c_2^2)(d-d_{\mathrm{SN}})$ and the coefficients f_i are given by

$$f_1 = \frac{2}{\alpha^2}, \quad f_2 = \frac{\alpha^2 + 12\alpha + 4}{\alpha^2}, \quad f_3 = \frac{4(\alpha^2 + 4\alpha + 4)}{\alpha}$$

with $\alpha \equiv \sqrt{1+c_2^2}$.

For $d > d_{\mathrm{SN}}$, the right hand side of Eq. (38) is negative, implying that $|\tilde{U}_-|^2 < V < |\tilde{U}_+|^2$. Combining this result with Eq. (37) enables us to conclude that for $d > d_{\mathrm{SN}}$, $\det(\mathbf{J}_+) < 0$, while $\det(\mathbf{J}_-) > 0$. Namely, $\tilde{U}_+$ is always a saddle, whereas

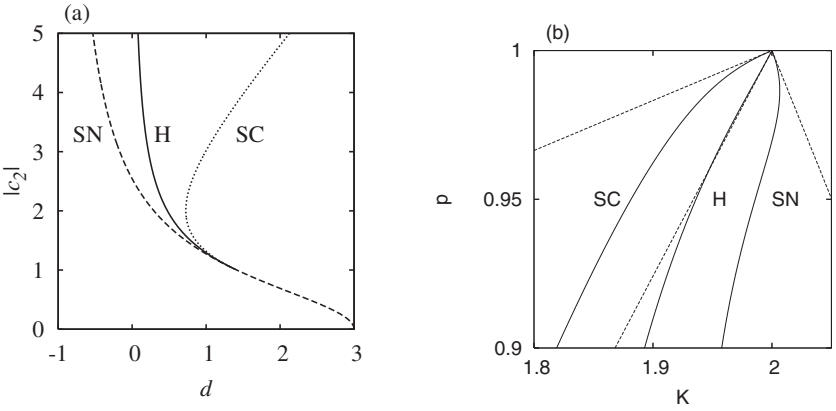

FIG. 6. The thresholds d_{SN},d_H, and d_{SC}. (a) Their c_2 dependence and (b) critical slopes due to them in comparison with numerically obtained bifurcation curves for $c_2=-3$, $a=2$, $b=1$. In (b), the straight lines (dotted) show the slopes of the bifurcation curves at the critical point $(K,p)=(K_c,1)=(2,1)$ obtained by the asymptotic analysis made in the text. In both panels, d_{SN} and d_H are due to Eqs. (35) and (39), respectively, while d_{SC} is due to direct simulation of Eq. (29).

$\tilde{U}_-$ is either a node or a focus. It is easy to show using Eqs. (32) and (36) that for $|c_2|<1$, $\tilde{U}_-$ remains to be an unstable node in the whole range of $d>d_{SN}$. In this case, there appear no attractors corresponding to the breakdown of synchronization of active oscillators. However, for $|c_2|>1$, it is stable in the range $d_{SN}<d<d_H$ and unstable for $d>d_H$, where

$$d_H \equiv \frac{1-c_2^2+\sqrt{4(1+c_2^2)+(1-c_2^2)^2}}{1+c_2^2}. \tag{39}$$

What happens for $d>d_H$ is qualitatively the same as what we have found for the $p=0$ case: $d=d_H$ is a Hopf bifurcation point, beyond which a stable limit-cycle appears until it disappears for some value of d, say d_{SC}, by colliding with the saddle $\tilde{U}_+$. For $d>d_{SC}$, there exist no attractors implying the desynchronization of active oscillators. The values of d_{SC} were evaluated by integrating Eq. (29) numerically. These analytical and numerical results for the critical values of d may be used to draw straight lines passing through $(K,p)=(K_c,1)$ which are tangent to corresponding bifurcation curves on the parameter plane, as demonstrated in Fig. 6(b). For example, the curve of saddle-node bifurcation has to be tangent to

$$K-a=a\left(1+\frac{a}{b}\right)d_{SN}(p-1) \tag{40}$$

at the critical point $(K,p)=(K_c,1)$ and likewise for the curves of Hopf bifurcation and saddle connection. It is important to note that for $|c_2|=1$, $d_H=d_{SN}(=\sqrt{2})$. In fact, our numerical results for d_{SC} as displayed in Fig. 6(a) suggest that all three critical values of d are the same for $|c_2|=1$, leaving only d_{SN} for $|c_2|$ smaller. Hence, just as in case (a), desynchronized attractors disappear for $|c_2|<1$ in the present case as well.

(c) *The remaining region and comparison with numerical results.* For the remaining region, we present only numerical results obtained from an analysis of Eq. (7) based on solutions of Eqs. (20)–(23) due to the Newton-Rapson method. The results cover all the region, as displayed in Fig. 1 [see also Fig. 6(b)]. We confirmed that the analytical results for cases (a) and (b) well agree with such results.

Let us recall that according to the present theory, two-cluster desynchronization of the active group with small size ratios can occur only in between the curve of the saddle connection and that of the saddle-node bifurcation. The whole region where desynchronized attractors exist in phase space will be probably larger than this. Nevertheless, when compared with the simulation results also displayed in Fig. 1, the curve of the saddle connection is found to nicely approximate the left boundary of the desynchronization horn. This fact is consistent with the observation that as K is increased, desynchronization starts with a two-cluster state with a small size ratio, as is seen in Fig. 3. In fact, we have confirmed that the trajectories of active oscillators belonging to the smaller cluster near the onset of clustering are nicely reproduced by the solution to Eq. (23). On the other hand, the curve of the saddle-node bifurcation is situated far away from the right boundary of the horn. This fact will be given an explanation from a different point of view in the next subsection. It should also be recalled that our analyses reveal that for both $p=0$ and $(K,p)-(K_c,1)$, the desynchronization of the active group as treated above does not happen if $|c_2|<1$. The numerical result, however, suggests that this holds everywhere on the (K,p) phase diagram [see Fig. 1(a)]. Although it is uncertain whether this is also true about other modes of desynchronization, these results explain, to some extent, the finding in simulation that the desynchronization horn disappears when $|c_2|$ is less than unity.

Before ending this subsection, we give some remarks. First, in the above, we have not discussed the stability of the clustering solutions in full phase space. The type of clustering discussed above is the small size-ratio limit of two-cluster states of the active group, so that the larger active cluster and the inactive group are virtually unaffected by the smaller active cluster. Therefore, as long as the synchronized state is stable as we have assumed on the basis of numerical results, the two-cluster states treated above that are stable in the subspace should also be stable in full phase space, in accordance with our numerical observations. Second, in cases (a) and (b) above, the fixed points born through saddle-node bifurcation come to possess double zero eigenvalues at the bifurcation point for $|c_2|=1$ [see Fig. 5 and Fig. 6(a)]. This is so called the Takens-Bogdanov degeneracy, near which it is known from a mathematically rigorous analysis that the three types of local and global bifurcations as found above take place [25]. Our analysis agrees with this. A similar kind of degeneracy occurs at the critical point $(K,p)=(K_c,1)$ in the phase diagrams for $|c_2|>1$, but it seems to be an exceptional one because unlike those just mentioned, the

three fixed points coalesce at the origin in this case, as can be seen from Eq. (8), though associated bifurcation structures appear to be the same. Finally, it should be noted that our theory developed here provides one natural scenario for the onset of quasiperiodicity in coupled identical oscillators. A different mechanism for such a phenomenon has been found recently for a population of oscillators coupled indirectly [26].

C. Swing-by mechanism of diffusion-induced inhomogeneity

In the foregoing subsections, by means of numerical simulation starting from random initial conditions, we have seen that the active group of the globally coupled system (2) exhibits clustering in a certain region of the (K,p) plane, dubbed the desynchronization horn. It has also been shown analytically that the simplest category of two-cluster states indeed exists in a region including the desynchronization horn, supporting in part the numerical observation. Instead of undertaking a study of other categories of desynchronization, we now turn our attention to other important issues of how random initial conditions lead to desynchronization and also how the degree of desynchronization or inhomogeneity of the system depends on parameters. These issues are related to a counterintuitive aspect of our findings reported above. In our model equations (2), the constituent oscillators are linked through diffusive couplings. This type of coupling is quite common in every subfield of nonlinear dynamics and, needless to say, its typical effect is to make the system uniform. There can be very interesting exceptions, however, when there is a substantial difference in diffusion constants (in a generalized sense) of the variables involved. For example, the well-known Turing instability refers to an instability of a spatially uniform state in reaction-diffusion systems occurring under such a situation [27]. Some neurophysiological models are also known to exhibit similar phenomena [28], where oscillators interact through diffusive couplings involving only one variable, i.e., membrane potential, and their synchronization breaks down as a result of cooperation between this one-variable coupling and strong nonisochronicity of the oscillators [29]. These examples demonstrate that diffusive coupling can counterintuitively induce inhomogeneity. Such an effect may be called diffusion-induced inhomogeneity.

It is important to notice that our system provides another example of diffusion-induced inhomogeneity. This may be already implicit in Fig. 1, but is shown more explicitly for the case of $p=0$ in Fig. 7, which presents simulation results for a measure of inhomogeneity of the system defined by

$$\sigma = \langle \overline{(|z_j - \bar{z}_j|^2)}^{1/2} \rangle, \tag{41}$$

where the overbars stand for averages over all oscillators and the brackets mean long-time average. The data in Fig. 7 are averages over ten different random initial conditions. Each data set indicates that in a range of K, the inhomogeneity of the system is enhanced by increasing K. This example of diffusion-induced inhomogeneity differs from the known ones at least in two crucial points: One is that in our model, the diffusive couplings are introduced symmetrically as to

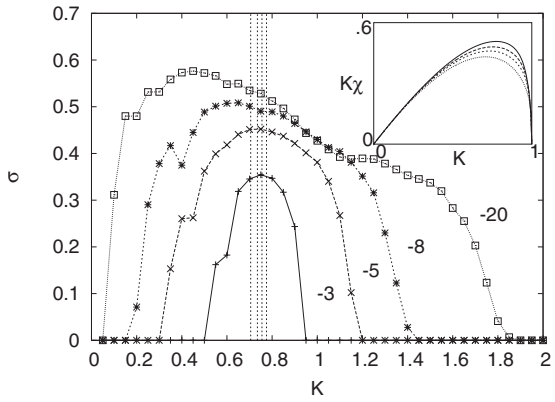

FIG. 7. The behavior of σ for $N=4000$ averaged over ten realizations of the random initial condition explained in the text. The numbers attached to the data are the values of c_2. The lines connecting the symbols are to guide the eye. The inset shows $K\chi$'s graphs in the range $0 \leqslant K \leqslant 1$, $0 \leqslant k\chi \leqslant 0.6$ for the same values of c_2, where its maximum values as well as its maximum points indicated by the vertical dotted lines in the main panel monotonically decrease for increasing $|c_2|$.

the two variables of each oscillator, namely the real and imaginary parts of its complex amplitude, and another is that the homogeneous state or the perfectly synchronized state remains stable even where the phenomenon takes place; in fact, a linear stability analysis in full phase space of the perfectly synchronized limit-cycle for $p=0$ (and $a=1$)

$$z_1 = \cdots = z_N = \exp\{i(-c_2 t + \text{const})\} \tag{42}$$

reveals that real parts of stability eigenvalues are in the set $-K,-2,-(K+2)$ except for zero, and hence, increasing K simply strengthens the stability of perfect synchronization. It will turn out below that the diffusion-induced inhomogeneity observed here originates from an interplay of random initial conditions and strong nonisochronicity of oscillators mediated by an incoherent state. This scenario remains essentially the same for $p>0$. Hereafter we fix the value of a at unity.

We first deal with the case of $p=0$ and then proceed to discuss the effect of aging $(p>0)$. Main results for the former were briefly reported in Ref. [15].

(a) The case of $p=0$. For convenience, let us rewrite Eq. (2) with $p=0$ in terms of polar coordinates

$$\dot{r}_j = (1 - K - r_j^2) r_j + KR \cos(\Theta - \theta_j), \tag{43}$$

$$\dot{\theta}_j = -c_2 r_j^2 + \frac{K}{N} \sum_{k=1}^{N} \frac{r_k}{r_j} \sin(\theta_k - \theta_j) \tag{44}$$

$$= -c_2 r_j^2 + \frac{K}{r_j} R \sin(\Theta - \theta_j), \tag{45}$$

where $z_j \equiv r_j e^{i\theta_j}$ and

$$Z \equiv \frac{1}{N}\sum_{k=1}^{N} z_k \equiv Re^{i\Theta}. \tag{46}$$

We first note that there is a simple category of exact solutions for the above equations, which are featured by the property $Z=0$ and called incoherent solutions [17–19]:

$$r_j = \sqrt{1-K}, \quad \theta_j = -c_2(1-K)t + \psi_j \tag{47}$$

for $1 \leqslant j \leqslant N$ and $0 < K < 1$ with constants ψ_j satisfying

$$\sum_{j=1}^{N} e^{i\psi_j} = 0. \tag{48}$$

Each of these solutions represents a state in which all the complex amplitudes lie on the circle with radius $\sqrt{1-K}$ in the complex plane, which circle will be hereafter referred to as the "incoherent circle." The variety of such solutions is actually very rich, because there is only one constraint on the large number of phase constants ψ_j [see Eq. (48)]. Here we focus on those solutions whose complex amplitudes are uniformly distributed on the incoherent circle. According to a linear stability analysis, such solutions are always unstable in the system studied in this paper (see the Appendix). However, they are of saddle type, possessing stable directions, as can be realized straightforwardly without invoking any stability analysis [15]. In fact, Eq. (2) is symmetric for the transformations $z_j \to -z_j$, so that for any trajectory of the system in full phase space starting from a set of initial complex amplitudes having the same symmetry, the mean field Z remains to be zero for all $t \geqslant 0$ and hence the trajectory will converge to an incoherent solution of the form (47) and (48). In other words, the whole set of reflection-symmetric points in phase space of Eq. (2) belongs to the stable manifold of "incoherence." If the initial complex amplitudes are in addition random enough so that their phase distribution is uniform, then the final incoherent state should be of the category on which we focus here. For the time being, we suppose that the initial state of the system is approximately of this type. In our numerical simulations, this is realized by setting the initial values of the complex amplitudes randomly in the range

$$-1 < \mathrm{Re}(z_j), \quad \mathrm{Im}(z_j) < 1, \tag{49}$$

as already mentioned. The initial value of R is then as small as $O(1/\sqrt{N})$, so that for some time thereafter, the system will approach an incoherent state, keeping its phase distribution almost uniform. Actually, at least qualitatively, the behavior of σ is not very sensitive to the degree of how well the initial condition satisfies the above requirements, in particular, when the nonisochronicity of the oscillators measured by $|c_2|$ is sufficiently strong (see below).

We then note that as the complex amplitudes approach the incoherent circle, their phases tend to be governed more and more by the Kuramoto model of identical phase oscillators [2]

$$\dot{\theta}_j = -c_2(1-K) + \frac{K}{N}\sum_{k=1}^{N} \sin(\theta_k - \theta_j), \tag{50}$$

according to Eq. (44). Moreover, in this regime, we see that R is roughly equal to $r_{\mathrm{IC}}Q = \sqrt{1-K}Q$, where r_{IC} is the radius of the incoherent circle and

$$Q \equiv \left| \frac{1}{N}\sum_{k=1}^{N} e^{i\theta_k} \right| \tag{51}$$

is the order parameter measuring phase coherence. Since the model (50) is known to synchronize for $K > 0$, the value of Q will start to increase when the original system comes close enough to an incoherent state, and this in turn will drive the system off such a state, since the second term on the right hand side of Eq. (43) becomes no longer negligible. This scenario is verified in Fig. 8. In panel (a) of this figure, the behavior of all r_j from $t=0$ is exemplified, indicating that the complex amplitudes initially tend to the incoherent circle, but then change directions to run away from it outward or inward, reflecting the fact that the sign of the second term on the right hand side of Eq. (43) depends on the oscillator phase. As Fig. 8(b) reveals, the oscillator phases θ_j remain almost uniformly distributed while the oscillators approach the incoherent circle, and then some coherence develops through the synchronization mechanism explained above, resulting in a rapid growth of R as displayed in Fig. 8(c) and hence in the departure of the oscillators from the incoherent circle. Of course, scattering of oscillator trajectories only in the radial direction is not enough to cause clustering; in fact, if the phases remain synchronized sufficiently well, the diffusive coupling will eventually drive the system into perfect synchronization. It is at this stage that the nonisochronicity of the oscillators plays a crucial role. A look at Eq. (44) shows that the effective natural frequency of the jth oscillator is given by $-c_2 r_j^2$. Hence, if $|c_2|$ is sufficiently large, the scattering in the radial direction will give rise to large dispersion in those effective frequencies, whereby the whole population should be strongly twisted along the azimuthal direction and as a result split into, roughly speaking, two groups characterized by large and small amplitudes. In this way, the system is expected to settle down in persistent desynchronization.

Recall that the degree of inhomogeneity σ behaves in a resonant way (see Fig. 7). We may ask why this happens and if it is possible to predict where σ becomes maximum. To answer these questions in a heuristic way, we recall that the growth of phase coherence triggers the clustering process through the phase-dependent term of Eq. (43). The key is therefore how the amplitude of that term KR depends on the phase order parameter Q. Our foregoing argument suggests that the stronger this dependence is, the more strongly the system is driven into splitting and thus inhomogeneity. Since the estimate $R \sim \sqrt{1-K}Q$ mentioned before is too crude, we exploit the linear stability analysis of the incoherent state to obtain

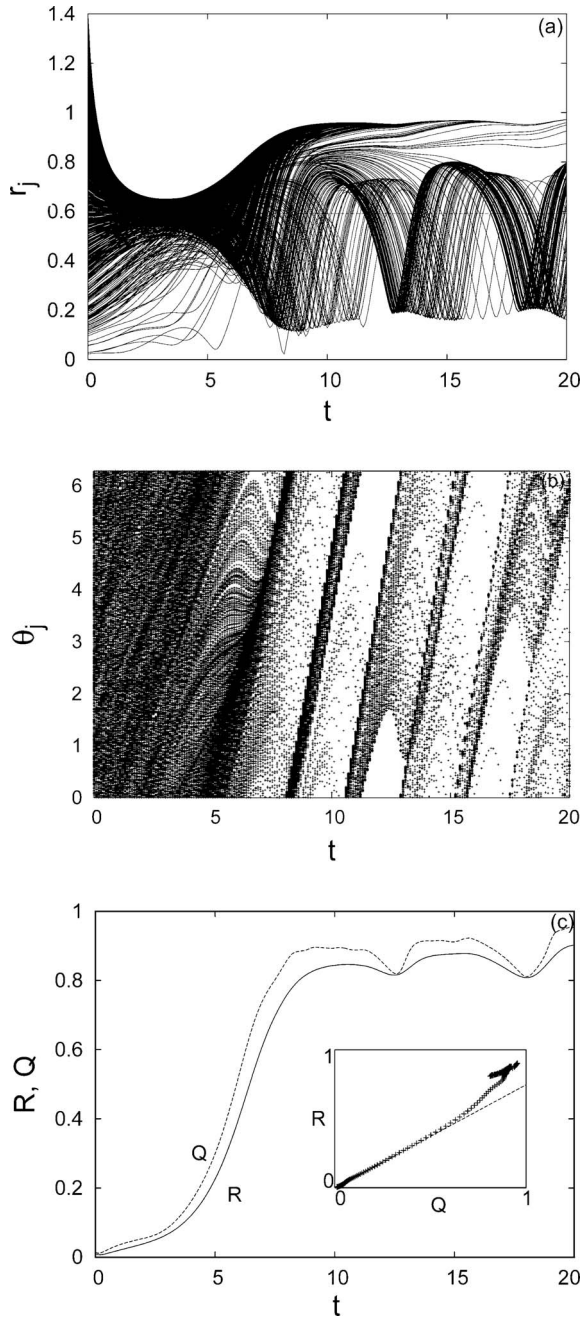

FIG. 8. Relaxation from a random initial condition for $c_2=-3$, $K=0.65$, $N=1000$. (a) Temporal behavior of $r_j \equiv |z_j|$, where the thin horizontal line shows the radius of the incoherent circle. (b) Likewise for $\theta_j \equiv \mathrm{Arg}(z_j)$. (c) The behavior of the order parameters R and Q, where the inset covers the ranges $0<Q,R<1$, demonstrating a fairly good agreement between the data and the predicted relationship $R=\chi Q$ as drawn with the broken line.

$$\frac{R}{Q} = \left| \frac{2(1-K)^{3/2}(1+ic_2)}{2(1-K)(1+ic_2)-K+\lambda} \right| \equiv \chi \qquad (52)$$

(see the Appendix), where λ is a stability eigenvalue of the incoherent state with the largest real part. The inset of Fig. 8(c) evidentiates that this approximation holds in a fairly wide range of Q. It thus turns out that in good approximation, KR is proportional to Q with the proportionality constant $K\chi$, which will govern the behavior of σ together with c_2. A number of $K\chi$ vs K plots with c_2 fixed are presented in the inside panel of Fig. 7, each showing a sharp resonancelike behavior with the maximum points agreeing fairly well with those of σ, as expected [30]. The reason why $K\chi$ and hence σ exhibit the resonancelike behavior may be considered here. For simplicity, we do this within the crude approximation of setting $K\chi$ to Kr_{IC}. As K is increased, the first factor K, which comes directly from the diffusive coupling, of course, increases, whereas the second factor $r_{\mathrm{IC}}=\sqrt{1-K}$ monotonically decreases. The "resonance" of σ is caused by competition between these two opposing effects of increasing the coupling strength on the magnitude of the clustering-triggering force. As a matter of fact, it is possible to show by using the equation of λ, (A15) with $p=0$ (see Appendix), that χ approaches r_{IC} for increasing $|c_2|$. Reflecting this fact, the maximum point of Kr_{IC}, i.e., $K=2/3$, makes a not so bad estimate of σ's peak point (see Fig. 7).

Actually, there are two problems to be resolved with the above heuristic explanation of the diffusion-induced inhomogeneity resonance. One is that it apparently cannot explain the inhomogeneity observed in the region $K>1$ where the incoherent circle no longer exists (see Fig. 7). In fact, this is a finite-size effect, because if the system is sufficiently large for each value of $K>1$, then the complex amplitudes are expected to come too close to one another to remain desynchronized during the initial stage in which all of them tend to the origin, as can be seen from Eq. (43) with $R=0$. In order to check this hypothesis, we examined the behavior of the system when initial complex amplitudes are distributed uniformly in a disc centered at the origin, finding that the system indeed falls in perfect synchronization for sizes of the disc smaller than a threshold value, say r_c. Owing to the symmetry of the system pointed out before, we can then expect that there is a critical system size $N_c<\infty$ such that the above condition is met at the initial stage if $N>N_c$. According to our simulation results, r_c increases as K grows and decreases as $|c_2|$ grows (data not shown). This result is consistent with the behavior of σ displayed in Fig. 7 which indicates that synchronization is easier for K larger and for $|c_2|$ smaller. Another problem is that the prediction for the maximum point of σ does not work very well when $|c_2|$ is too large, as is clear in Fig. 7. This is because excessive nonisochronicity breaks the swing-by scenario by confining the oscillators to a neighborhood of the incoherent circle. Namely, as soon as the oscillators leave the incoherent circle, so big frequency differences are generated that they quickly spread along the circle, thereby the value of R being rapidly reduced back towards zero, and therefore the oscillators making U-turns to approach the incoherent circle again [31]. The first two panels of Fig. 9 demonstrate that this process is repeated on and on and that at each cycle, the size ratio between the large amplitude and small amplitude groups varies in a complicated way. Consequently, as Fig. 9(c) indicates, R is no longer proportional to Q, so that there is no reason why the theoretical estimate of the peak point of σ works very well. The repeated process tends to fatten the smaller group and make the oscillation amplitudes of R and Q bigger than when the nonisochronicity is moderately strong.

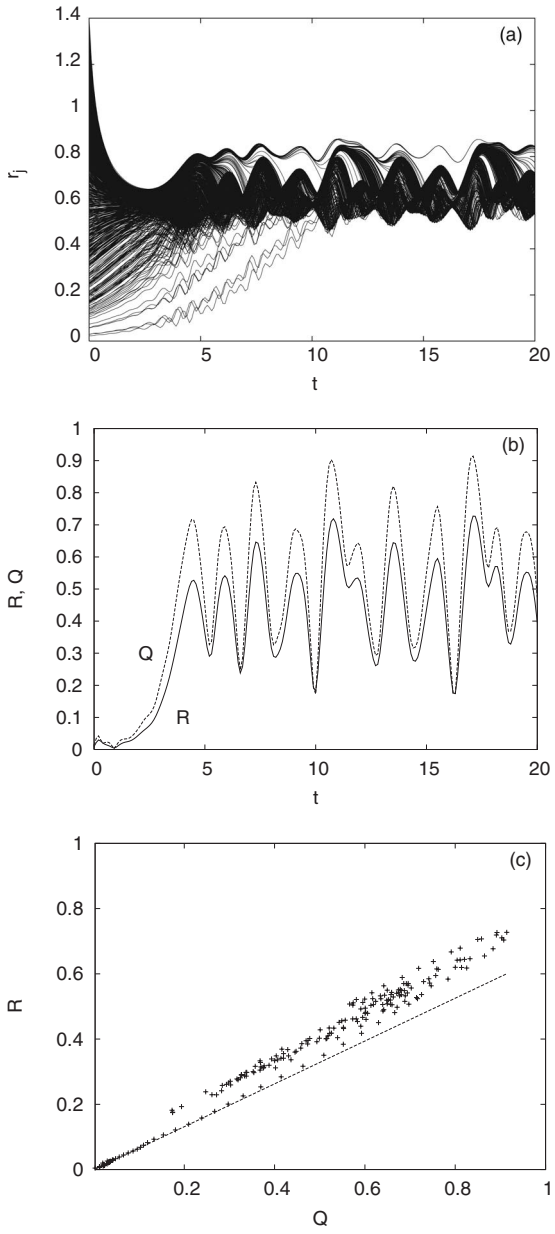

FIG. 9. Relaxation from a random initial condition for $c_2=-20$, $K=0.65$, $N=1000$. (a) Temporal behavior of $r_j \equiv |z_j|$, where it should be noted that the radius of the incoherent circle is $\sqrt{1-K}=0.5916,\ldots$, which is the same as in Fig. 8(a). (b) Corresponding behaviors of R and Q. (c) R vs Q in the relaxation process of (a), where the dotted line shows $R=\chi Q$.

(b) The case of $0<p<1$. The effect of aging on diffusion-induced inhomogeneity can be analyzed in a similar way. The role of incoherent states is here played by such states that

$$z_j = \sqrt{1-K}e^{i\theta_j} \quad (j \in S_a),$$

$$= 0 \quad (j \in S_i), \tag{53}$$

where the phases θ_j have the same form as Eq. (47) with constants ψ_j satisfying $\Sigma_{j\in S_a} e^{i\psi_j}=0$. According to numerical simulation, the inactive oscillators always remain synchronized, so that here we pay attention only to the inhomogeneity of the active group and introduce its standard deviation σ_a as Eq. (41) with the overbar meaning an average over all $j \in S_a$. Similarly, we introduce the phase order parameter of the active group Q_a. Then, since the equation of r_j for each active oscillator is the same as before, a good measure of the strength of the splitting force will be given by $K\chi_a \equiv KR/Q_a$. A linear stability analysis of the generalized incoherent states (53) yields the following formula:

$$K\chi_a = 2(1-p)K\sqrt{1-K}\left|\frac{\lambda + K + b - ic_2(1-K)}{\lambda + K(1-p) + b - ic_2(1-K)}\right| \times \left|\frac{\lambda + (1-K)(1-ic_2)}{\lambda + 2(1-K)(1-ic_2)}\right|, \tag{54}$$

where λ is a linear stability eigenvalue of the incoherent state with the largest real part (see the Appendix for details).

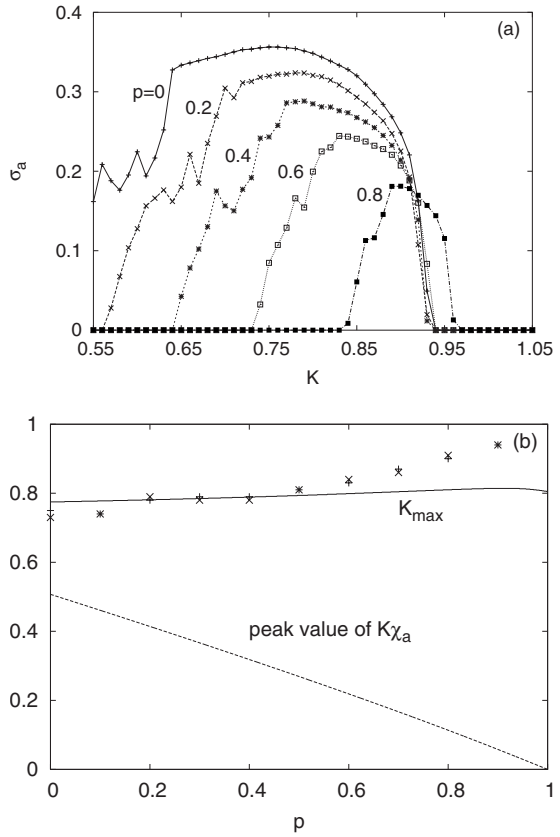

FIG. 10. Behavior of σ_a: p dependence and comparison with theory. Symbols show simulation results for $N=4000$, $c_2=-3$, $a=b=1$ averaged over ten different random initial conditions. (a) σ_a vs K for the five values of p indicated. (b) p dependence of $K_{\max}$ defined as the maximum point of σ_a for p fixed; the real curve is due to theory, while two of the symbols show simulation results for two runs. The broken curve shows the peak value of K_{χ_a} for each fixed value of p.

Figure 10(a) shows the behavior of σ_a obtained by simulation for several values of p, where the level of inhomogeneity is seen to monotonically go down as the aging proceeds, though σ_a does not change its behavior qualitatively. This result may be explained from our theory, because the

maximum value of $K\chi_a$ computed from Eq. (54) also decreases for increasing p, as demonstrated in Fig. 10(b). The above formula of K_{χ_a} enables us to predict the maximum point of σ_a, as before, by calculating the value of K at which K_{χ_a} is largest for each fixed value of p. The upper curve in Fig. 10(b) shows the result, indicating that this prediction is good for p less than roughly 0.6, but not very efficient for p larger. This is not surprising, because when p is large, the resonance of K_{χ_a} is no longer sharp and almost disappears [data not shown, but this may be guessed from the behavior of the maximum value of K_χ displayed in Fig. 10(b)]. Figure 10 only provides the results for $c_2=-3$, but we found similar results for $c_2=-5$ as well.

Note that in the mechanism discussed in the present subsection, each oscillator behaves in a way reminiscent of the swing-by motion of a space explorer, in which it is first attracted by a star and then redirected for its destination star; the role of the incoherent circle is analogous to that of the first star. This is why we call the present mechanism of diffusion-induced inhomogeneity the swing-by mechanism.

D. Strong damping limit

This final subsection is devoted to a study of a limiting case such that the damping of the inactive oscillators is strong, namely, $b \gg K$. As we see below, the effect of aging on globally coupled Stuart-Landau oscillators is then much more tractable than otherwise. Let us start by recalling the original equations: for $j \in S_a$,

$$\dot{z}_j = (1-K)z_j - (1+ic_2)|z_j|^2 z_j + \frac{K}{N}\sum_{k=1}^{N} z_k \tag{55}$$

and for $j \in S_i$,

$$\dot{z}_j = (-b-K)z_j - (1+ic_2)|z_j|^2 z_j + \frac{K}{N}\sum_{k=1}^{N} z_k. \tag{56}$$

The basic idea is simple: Under the assumption on the damping rate b, we can safely put $z_j \sim 0$ for every inactive oscillator. The active oscillators may then be thought of as independent of them and hence obeying

$$\dot{z}_j = (1-K)z_j - (1+ic_2)|z_j|^2 z_j + \frac{K(1-p)}{N_a}\sum_{k=1}^{N_a} z_k, \tag{57}$$

where $N_a \equiv (1-p)N$ is the number of the active components of the system. Assuming that $1-Kp>0$ and introducing the set of transformations

$$A_j \equiv \frac{z_j}{\sqrt{1-Kp}}, \tag{58}$$

$$\tau \equiv (1-Kp)t, \tag{59}$$

$$K_a \equiv \frac{K(1-p)}{1-Kp}, \tag{60}$$

we obtain from Eq. (55)

$$\frac{dA_j}{d\tau} = A_j - (1+ic_2)|A_j|^2 A_j + \frac{K_a}{N_a}\sum_{k=1}^{N_a}(A_k - A_j), \tag{61}$$

which is nothing but the agingfree version (i.e., $p=0$) of our original equations (2) except that both the system size and the coupling strength instead depend on the aging level p. Note that c_2 remains the same. A useful implication follows from this correspondence: Suppose that in the original system (2) with $p=0$, a bifurcation phenomenon takes place at a certain value of K; this value may vary with the system size, so that we write it $K_0(N)$. Then, owing to Eqs. (58)–(61), the same phenomenon will occur in the active group of the aged system with the aging level p $(0<p<1)$ at the coupling strength given by

$$K = \frac{K_0(N_a)}{1-p[1-K_0(N_a)]}. \tag{62}$$

This formula simplifies for the infinite-size system as

$$K = \frac{K_0(\infty)}{1-p[1-K_0(\infty)]}. \tag{63}$$

Note that these formulas do not violate the initial assumption $1-Kp>0$, as easily confirmed, so that the consistency of our argument is maintained. Note also that the right-hand sides of Eqs. (62) and (63) converge to unity for $p \to 1$. This fact may suggest that all bifurcation sets lying on the (K,p) plane accumulate at the critical point, $(K,p)=(K_c,1)=(1,1)$, at least in the strong damping limit.

As examples, let us take the saddle-node, Hopf, and saddle-connection bifurcations in two-cluster states in the small size-ratio limit as discussed in Sec. II B. Formula (63) tells that for each value of p, corresponding bifurcations occur in the active group at

$$K = K_\#(p) \equiv \frac{K_\#}{1-p(1-K_\#)}, \tag{64}$$

where the subscript $\# \in \{\mathrm{SN},\mathrm{H},\mathrm{SC}\}$ and $K_\#$ on the right hand side means corresponding bifurcation points in the agingfree system. Figure 11 compares these with numerical results for $b=5$. We find that they are in nice agreement even for this moderately large value of b.

III. OTHER EXAMPLES OF COUPLED LIMIT-CYCLE OSCILLATORS

In the preceding section, we have found that the (K,p) phase diagram of globally and diffusively coupled Stuart-Landau oscillators with $|c_2|>1$ has a horn-shaped region converging at $(K,p)=(K_c,1)$ in which active oscillators are desynchronized for random initial conditions in a way which can be viewed as a type of diffusion-induced inhomogeneity. The aim of this section is to find out how general the existence of such a region, the desynchronization horn, is in the (K,p) phase diagrams of globally and diffusively coupled limit-cycle oscillators other than the coupled Stuart-Landau systems. The desynchronization horn should come into existence at least if both active and inactive elements are in the

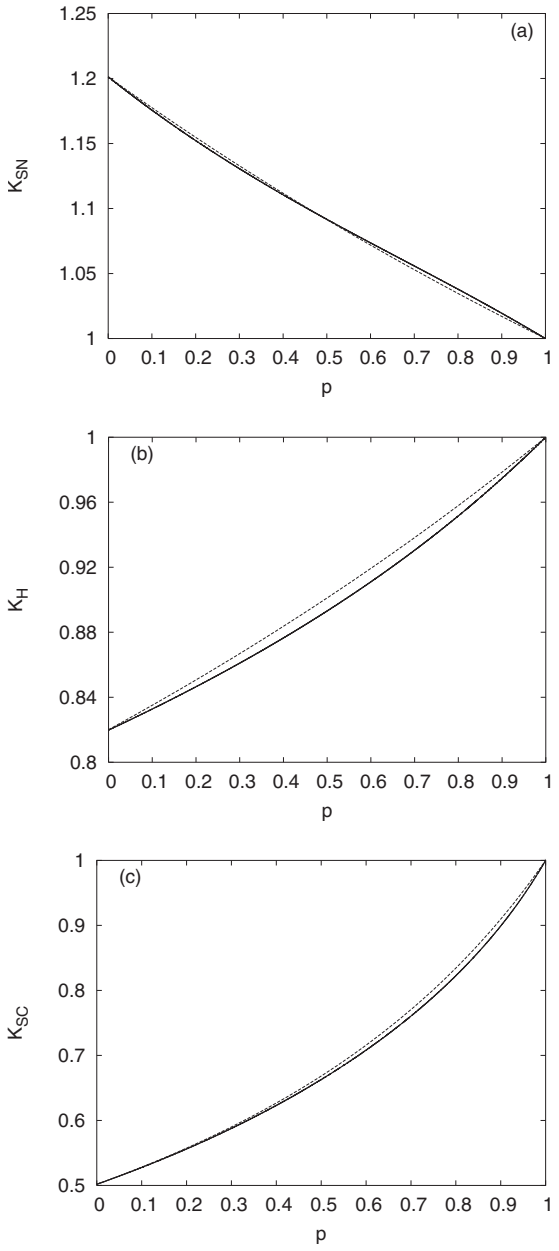

FIG. 11. Examination of the formula (64) for the bifurcation curves in the small size-ratio limit, where $b=5$; (a) K_{SN}, (b) K_H, (c) K_{SC}. In each panel, the solid and broken lines show numerical results based on the Newton-Rapson method and the formula, respectively.

neighborhood of a Hopf bifurcation and possess strong enough nonisochronicity, since the dynamics of the system then can be reduced to those of the coupled Stuart-Landau systems by a normal form analysis (to be exact, this requires an additional constraint such that the coupling in the original system is sufficiently weak). An example corresponding to this case is shown in Figs. 12(c) and 12(d) which are devoted to the coupled Brusselators [32]:

$$\dot{x}_j = A - (B_j + 1)x_j + x_j^2 y_j + \frac{K}{N}\sum_{k=1}^{N}(x_k - x_j), \tag{65}$$

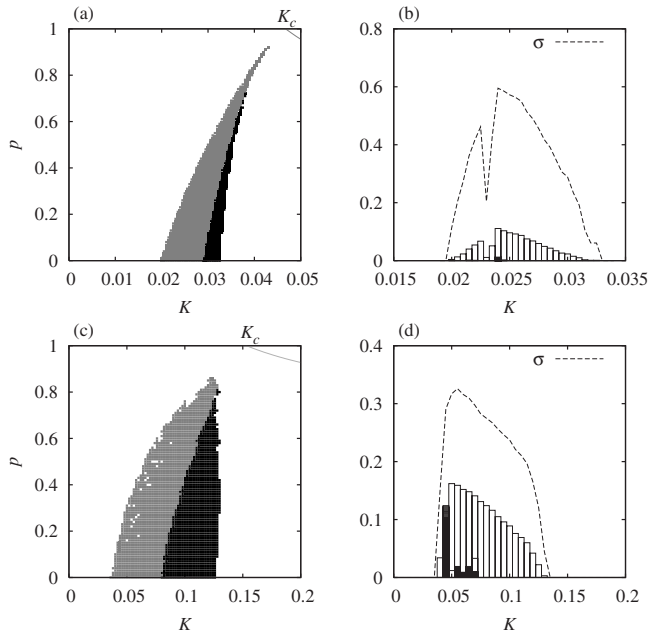

FIG. 12. Desynchronization horns and cluster structures found numerically for the coupled periodic Rössler systems (67)–(69) [(a), (b)] and the coupled Brusselators (65) and (66) [(c), (d)] where $N=1000$ in all panels, and $p=0$ in (b) and (d). The results in each panel were obtained for a random initial condition. Other details are the same as in Figs. 1 and 3.

$$\dot{y}_j = B_j x_j - x_j^2 y_j + \frac{K}{N}\sum_{k=1}^{N}(y_k - y_j), \tag{66}$$

where $A=3$ and $B_j=10.2$ $(j \in S_a), 9.8$ $(j \in S_i)$. Note that in an isolated Brusselator with A fixed, we have Hopf bifurcation at $B=B_c \equiv 1+A^2$, which equals 10 in the present case. According to Eq. (B.18b) of Ref. [2], we obtain $c_2=(4-7A^2+4A^4)/[3A(2+A^2)]=2.676\cdots>1$. The data in Fig. 12(c) indicate that the (K,p) phase diagram indeed has qualitatively the same structure as those of the coupled Stuart-Landau systems. This is also seen in Fig. 12(d), where the behavior of σ as well as the cluster structure are presented for $p=0$.

Our results displayed in Figs. 12(a) and 12(b) demonstrate, however, that the desynchronization horn and associated diffusion-induced inhomogeneity might be more common. Those panels are for coupled Rössler systems [33] of the form [12]

$$\dot{x}_j = -y_j - z_j + \frac{K}{N}\sum_{k=1}^{N}(x_k - x_j), \tag{67}$$

$$\dot{y}_j = x_j + c_j y_j + \frac{K}{N}\sum_{k=1}^{N}(y_k - y_j), \tag{68}$$

$$\dot{z}_j = d_j + z_j(x_j - e_j) + \frac{K}{N}\sum_{k=1}^{N}(z_k - z_j) \tag{69}$$

for $j=1,\ldots,N$, where $c_j=d_j=0.2$, $e_j=1$ $(j \in S_a)$, $c_j=d_j=-0.2$, $e_j=2.5$ $(j \in S_i)$; for $K=0$, each active element exhibits

periodic oscillation, while every inactive element falls into a fixed point. In spite that the parameter values defining both active and inactive oscillators are ad hoc chosen, the results are quite similar to those for the coupled Stuart-Landau systems. To conclude, the desynchronization horn and associated diffusion-induced inhomogeneity may be fairly general phenomena in populations of globally and diffusively coupled active and inactive oscillators.

IV. SUMMARY, REMARKS, AND REMAINING PROBLEMS

In this paper, we have discussed the effect of "aging" for populations of globally and diffusively coupled limit-cycle oscillators, focusing on the desynchronization of active oscillators which takes place inside a horn-shaped region (desynchronization horn) in the plane of the coupling strength K and the ratio of inactive oscillators p. By choosing the Stuart-Landau oscillators as a prototypic model of periodic oscillators, we have shown analytically and numerically that the desynchronization horn emerges only when the nonisochronicity of the oscillators (amplitude dependency of frequency) is sufficiently strong and that it has some characteristic features. This phenomenon can be interpreted as a type of diffusion-induced inhomogeneity, which, unlike already known types, relies on neither unequal coupling constants nor destabilization of the uniform (synchronized) state. We have found that it instead originates from an interplay between random initial conditions, the nature of coupling among oscillators (global and diffusive), and sufficiently strong nonisochronicity (the swing-by mechanism). Moreover, a theory has been developed to estimate the value of a control parameter at which the inhomogeneity of active oscillators becomes maximum. This theory has been found to be efficient for not too strong nonisochronicity and for p not very large, providing probably the first theoretical means to predict the degree of inhomogeneity of coupled oscillators, though further studies may be necessary to establish it. Our results for some other coupled oscillators (Rössler systems and Brusselators) suggest that these phenomena are not inherent to the coupled Stuart-Landau oscillators, but can be found in a wide class of periodic oscillators. It is therefore expected that in addition to the aging transition found in our earlier work [12], both the desynchronization horn and the diffusion-induced inhomogeneity based on the swing-by mechanism will be key concepts in the description of the aging of coupled periodic oscillators. Hopefully, the results of this paper will lead to some useful applications in the control of coupled-oscillator dynamics in such a situation that effects of bad components are unavoidable.

There remain a variety of interesting and important subjects. Here we name only a few. First, the complex structure of clustering near the maximum point of σ_a (Figs. 7 and 12) needs to be elucidated. Our theory developed in Sec. II B successfully reproduces some crucial features of the desynchronization horn, i.e., the hornlike shape converging at the critical point $(K,p)=(K_c,1)$ [34], the left boundary, and the transition between periodicity and nonperiodicity inside it, but this theory is restricted to the simplest category of desynchronization of the active group. It will be desirable to extend it to more general types of desynchronization or clustering and uncover the nature of the complexity in the central region of the horn. An interesting question in this connection is whether or not all bifurcation curves inside the active region $(p<p_c)$ accumulate at the critical point, just as found in the strong damping limit (Sec. II D). Second, the diffusive coupling considered in this paper is confined to the scalor type. Such a coupling can be realized in experiments of chemical reactors such that each pair of reactors are bidirectionally coupled with peristaltic pumps [35], where the strengths of diffusive coupling thus created are the same for all chemical species involved, and probably in many other experiments. However, for the sake of generality, it may be examined what happens if the constraint of the scalor type is relaxed, for example, by making K complex in the case of the coupled Stuart-Landau oscillators. Third, the effect of nonidenticality of oscillators in each subgroup will be worth extensive studies from a practical point of view. Last but not least, it will be of significance to clarify biological or physiological implications of the results in this work. These and other problems will be discussed elsewhere.

ACKNOWLEDGMENTS

The authors thank T. Horita, T. Mizuguchi, H. Fukuta, and other members of their nonlinear physics group for valuable discussions. This work was supported by the Grant-in-Aid for Scientific Research from the Ministry of Education, Culture, Sports, Science, and Technology.

APPENDIX: THE SPECTRUM OF STABILITY EIGENVALUES OF THE INCOHERENT STATE AND THE DERIVATION OF EQS. (54) AND (52)

The generalized incoherent solutions, which exist for $0<K<1$, may be expressed as

$$z_j=\sqrt{1-K}e^{i(\omega t+\psi_j)}\equiv z_j^{(0)} \quad (j\in S_a) \tag{A1}$$

$$=0 \quad (j\in S_i), \tag{A2}$$

where $\omega\equiv -c_2(1-K)$ and ψ_j in (A1) are phase constants such that $\Sigma_{j\in S_a}e^{i\psi_j}=0$. Since incoherent solutions relevant to our study are those whose phase distributions are uniform on the incoherent circle, we impose another constraint on ψ_j: $\Sigma_{j\in S_a}e^{2i\psi_j}=0$. For convenience, we extend the definition of $z_j^{(0)}$ over $j\in S_i$ as it is in Eq. (A1) but with arbitrary constants ψ_j. Let us consider the linear stability of such a solution by introducing perturbation variables u_j as

$$z_j=(1+u_j)z_j^{(0)} \quad (j\in S_a), \tag{A3}$$

$$=u_j z_j^{(0)} \quad (j\in S_i), \tag{A4}$$

whose substitution into Eq. (2) with $a=1$ leads to

$$\dot{u}_j=[-(1-K)+i\omega]u_j-(1-K)(1+ic_2)u_j^* + \frac{K}{N}\sum_{k=1}^{N}e^{i(\psi_k-\psi_j)}u_k \quad (j\in S_a), \tag{A5}$$

$$\dot{u}_j = [-(b+K) - i\omega]u_j + \frac{K}{N}\sum_{k=1}^{N} e^{i(\psi_k - \psi_j)}u_k \quad (j \in S_i), \tag{A6}$$

where the asterisk stands for complex conjugate. In order to find stability eigenvalues of the incoherent solution, we pay attention to the fact that the three macrovariables

$$E \equiv \frac{1}{N(1-p)}\sum_{j\in S_a} e^{i\psi_j}u_j, \tag{A7}$$

$$F \equiv \frac{1}{N(1-p)}\sum_{j\in S_a} e^{i\psi_j}u_j^*, \tag{A8}$$

$$G \equiv \frac{1}{Np}\sum_{j\in S_i} e^{i\psi_j}u_j \tag{A9}$$

obey the following equations:

$$\dot{E} = [-1 + K(2-p) + i\omega]E - (1-K)(1+ic_2)F + KpG, \tag{A10}$$

$$\dot{F} = -(1-K)(1-ic_2)E + [-(1-K) - i\omega]F, \tag{A11}$$

$$\dot{G} = K(1-p)E + [-b - K(1-p) - i\omega]G. \tag{A12}$$

Note that $E=F=G=0$ constitutes an invariant subspace in the whole phase space of $\{u_j\}$, in which subspace we have

$$\dot{u}_j = [-(1-K) + i\omega]u_j - (1-K)(1+ic_2)u_j^* \quad (j \in S_a), \tag{A13}$$

$$\dot{u}_j = [-(b+K) - i\omega]u_j \quad (j \in S_i). \tag{A14}$$

From Eq. (A13), we obtain stability eigenvalues $\lambda=0$ and $-2(1-K)$, both of which are $[N(1-p)-2]$-fold degenerate, while from Eq. (A14) we obtain $\lambda=-(b+K)-i\omega$, which is $[2(Np-1)]$-fold degenerate. All these eigenvalues are either stable or marginally stable ($\mathrm{Re}\lambda \leqslant 0$).

Let us now go back to the evolution equations of the macrovariables, which describe perturbations transversal to the invariant subspace. It is quite easy to see that associated eigenvalues are given by $\lambda=-b-K(1-p)-i\omega$ as well as

$$\lambda^2 - [K(3-p)-2]\lambda - K(1-K)(1-p)(1-ic_2) = 0. \tag{A15}$$

Note that the spectrum of stability eigenvalues for the incoherent solution is completed by adding complex conjugates of these eigenvalues. Let the roots of Eq. (A15) be λ_+ and λ_- with $\mathrm{Re}\lambda_+ > \mathrm{Re}\lambda_-$. Since it is possible to prove that $\mathrm{Re}\lambda_+\mathrm{Re}\lambda_- \leqslant -K(1-K)(1-p)$, we see that $\mathrm{Re}\lambda_+ > 0$ as well as $\mathrm{Re}\lambda_- < 0$ for the region $0<K<1, 0<p<1$ treated here. Hence it turns out that among all the stability eigenvalues of the incoherent solution, only λ_+ and its complex conjugate are unstable. Anyway, this establishes that the incoherent state is linearly unstable.

We now derive the formula of $K\chi_a$ (54). Noting that the mean-field Z and the phase order parameter of the active group Q_a are, respectively, given by

$$Z \equiv \frac{1}{N}\sum_{j=1}^{N} z_j = \sqrt{1-K}e^{i\omega t}[(1-p)E + pG] \tag{A16}$$

and

$$Q_a \equiv \left|\frac{1}{N(1-p)}\sum_{j\in S_a} e^{i\theta_j}\right| = \left|\frac{1}{N(1-p)}\sum_{j\in S_a}\frac{1+u_j}{|1+u_j|}e^{i\psi_j}\right| \cong \left|\frac{1}{2}(E-F)\right|, \tag{A17}$$

where higher order terms are ignored, we arrive at

$$\frac{|Z|}{Q_a} \cong 2\sqrt{1-K}\left|\frac{(1-p)E + pG}{E-F}\right| \equiv \chi_a. \tag{A18}$$

In the swing-by process, the system approaches an incoherent state sufficiently closely and eventually leaves it along the unstable direction found above. Therefore, in the latter stage, we may consider (E,F,G) as proportional to the eigenvector corresponding to the eigenvalue λ_+. We thus obtain from Eqs. (A7)–(A9)

$$\frac{F}{E} = \frac{-(1-K)(1-ic_2)}{\lambda_+ + (1-K) + i\omega}, \tag{A19}$$

$$\frac{G}{E} = \frac{K(1-p)}{\lambda_+ + b + K(1-p) + i\omega}. \tag{A20}$$

Substitution of these into Eq. (A18) leads to the formula of $K\chi_a$ (54) in which λ should read λ_+ in the notation here. By taking the limit $p\to 0$, we obtain an expression of χ which can be shown to be equivalent to Eq. (52).

[1] A. T. Winfree, J. Theor. Biol. **16**, 15 (1967).
[2] Y. Kuramoto, *Chemical Oscillations, Waves, and Turbulence* (Springer, Berlin, 1984).
[3] H. Daido, Int. J. Bifurcation Chaos Appl. Sci. Eng. **7**, 807 (1997).
[4] S. H. Strogatz, Physica D **143**, 1 (2000).
[5] J. A. Acebrón, L. L. Bonilla, C. J. P. Vicente, F. Ritort, and R. Spigler, Rev. Mod. Phys. **77**, 137 (2005).
[6] A. T. Winfree, *The Geometry of Biological Time* (Springer, New York, 2001).
[7] A. K. Engel, P. König, A. K. Kreiter, T. B. Schillen, and W. Singer, Trends Neurosci. **15**, 218 (1992).
[8] K. Wiesenfeld, P. Colet, and S. H. Strogatz, Phys. Rev. Lett. **76**, 404 (1996).

[9] I. Z. Kiss, Y. Zhai, and J. L. Hudson, Science **296**, 1676 (2002).
[10] K. Miyakawa and K. Yamada, Physica D **151**, 217 (2001).
[11] H. Fukuda, J. Kodama, and S. Kai, BioSystems **77**, 41 (2004).
[12] H. Daido and K. Nakanishi, Phys. Rev. Lett. **93**, 104101 (2004).
[13] K. Nakanishi and H. Daido, Prog. Theor. Phys. Suppl. **161**, 173 (2006).
[14] D. Pazó and E. Montbrio, Phys. Rev. E **73**, 055202(R) (2006).
[15] H. Daido and K. Nakanishi, Phys. Rev. Lett. **96**, 054101 (2006).
[16] M. Shiino and M. Frankowicz, Phys. Lett. A **136**, 103 (1989).
[17] P. C. Matthews, R. E. Mirollo, and S. H. Strogatz, Physica D **52**, 293 (1991).
[18] V. Hakim and W.-J. Rappel, Phys. Rev. A **46**, R7347 (1992).
[19] N. Nakagawa and Y. Kuramoto, Prog. Theor. Phys. **89**, 313 (1993).
[20] A. Pikovsky, M. Rosenblum, and J. Kurths, *Synchronization-A Universal Concept in Nonlinear Sciences* (Cambridge University Press, Cambridge, 2001).
[21] M. Tachikawa (unpublished).
[22] D. Golomb, D. Hansel, B. Shraiman, and H. Sompolinsky, Phys. Rev. A **45**, 3516 (1992).
[23] K. Okuda, Physica D **63**, 424 (1993).
[24] The linear stability of this solution was confirmed by numerically computing Floquet exponents for several values of c_2 in the range $0<p<p_c$, $0<K<2K_c$.
[25] J. Guckenheimer and P. Holmes, *Nonlinear Oscillations, Dynamical Systems, and Bifurcations of Vector Fields* (Springer, New York, 1983).
[26] M. Rosenblum and A. Pikovsky, Phys. Rev. Lett. **98**, 064101 (2007).
[27] J. D. Murray, *Mathematical Biology* (Springer, Berlin, 1993).
[28] A. Sherman and J. Rinzel, Proc. Natl. Acad. Sci. U.S.A. **89**, 2471 (1992).
[29] S. K. Han, C. Kurrer, and Y. Kuramoto, Phys. Rev. Lett. **75**, 3190 (1995).
[30] Note that the splitting (desynchronizing) force depends on not only $K\chi$ but also $|c_2|$. Since the dispersion of the effective natural frequencies is proportional to $|c_2|$, increasing $|c_2|$ will intensify the force and hence enhance the inhomogeneity of the system. This explains why the value of σ grows as $|c_2|$ is increased, as seen in Fig. 7. Although the value of $K\chi$ tends to decrease for increasing $|c_2|$ (see the inset of Fig. 7), such a change is relatively small and hence does not affect the behavior of σ in a qualitative way.
[31] This sticking of oscillator trajectories to the incoherent circle, which is enhanced by increasing $|c_2|$, provides a possible reason why the peak of σ shifts to the small K side as $|c_2|$ grows, as Fig. 7 indicates. This is because in the limit of strong sticking, σ should be approximated by $r_{\mathrm{IC}}=\sqrt{1-K}$ and hence become maximum near $K=0$.
[32] I. Prigogine and R. Lefever, J. Chem. Phys. **48**, 1695 (1968).
[33] O. E. Rössler, Phys. Lett. **71**, 155 (1979).
[34] This may imply that the scaling law of an order parameter proposed in our earlier paper [12] does not hold over a full range of the scaling variable, since it is based on the assumption that both the active and inactive groups are synchronized [12]. However, the scaling law is about a close vicinity of the critical point, where the horn is quite thin, unless the nonisochronicity of oscillators is extremely strong. One can therefore expect that it practically holds even if a desynchronization horn exits. Of course, if the stably coexisting synchronized state is traced from outside the horn, then no violation of the scaling law will occur at all.
[35] M. Yoshimoto, K. Yoshikawa, and Y. Mori, Phys. Rev. E **47**, 864 (1993).